ACS APPLIED MATERIALS & INTERFACES

Research Article

Cite This: ACS Appl. Mater. Interfaces 2018, 10, 23501−23508

www.acsami.org

Label-Free Graphene Oxide-Based Surface Plasmon Resonance Immunosensor for the Quantification of Galectin-3, a Novel Cardiac Biomarker

Emiliano N. Primo,[†,‡] Marcelo J. Kogan,[§] Hugo E. Verdejo,[∥] Soledad Bollo,[*,§] María D. Rubianes,[*,†,‡] and Gustavo A. Rivas[*,†,‡]

[†]INFIQC (CONICET), Haya de la Torre s/n, Ciudad Universitaria, X5000HUA Córdoba, Argentina

[‡]Departamento de Fisicoquímica, Facultad de Ciencias Químicas, Universidad Nacional de Córdoba, Ciudad Universitaria, X5000HUA Córdoba, Argentina

[§]Advanced Center for Chronic Diseases (ACCDiS), Facultad de Ciencias Químicas y Farmacéuticas, Departamento de Química Farmacológica y Toxicológica, Universidad de Chile, 8380492 Santiago, Chile

[∥]Advanced Center for Chronic Diseases (ACCDiS), División de Enfermedades Cardiovasculares, Facultad de Medicina, Pontificia Universidad Católica de Chile, 7500011 Santiago, Chile

Supporting Information

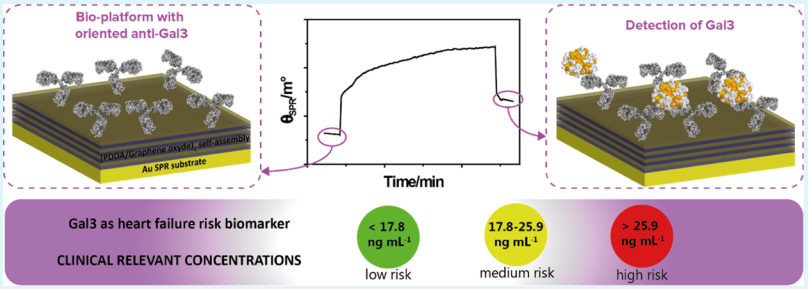

ABSTRACT: We report the first optical biosensor for the novel and important cardiac biomarker, galectin-3 (Gal3), using the anti-Gal3 antibody as a biorecognition element and surface plasmon resonance (SPR) for transducing the bioaffinity event. The immunosensing platform was built at a thiolated Au surface modified by self-assembling four bilayers of poly-(diallyldimethylammonium chloride) and graphene oxide (GO), followed by the covalent attachment of 3-aminephenylboronic acid (3ABA). The importance of GO, both as the anchoring point of the antibody and as a field enhancer for improving the biosensor sensitivity, was critically discussed. The advantages of using 3ABA to orientate the anti-Gal3 antibody through the selective link to the Fc region were also demonstrated. The new platform represents an interesting alternative for the label-free biosensing of Gal3 in the whole range of clinically relevant concentrations (linear range between 10.0 and 50.0 ng mL^{-1}, detection limit of 2.0 ng mL^{-1}) with successful application for Gal3 biosensing in enriched human serum samples.

KEYWORDS: *galectin3, immunosensor, SPR, graphene oxide, cardiac biomarker, layer-by-layer self-assembly*

1. INTRODUCTION

Heart failure (HF) is a complex clinical syndrome that occurs when the heart is unable to pump an adequate amount of blood. Despite the efforts in prevention, HF is a growing epidemic associated with staggering morbidity, mortality, and health costs. Currently, the estimated prevalence of HF exceeds 23 million people worldwide.[1] Despite its epidemiological relevance, the diagnosis of HF is challenging because its symptoms are often nonspecific, and physical examination can be misleading. The gold standard techniques such as echocardiography require a well-trained operator and equipment, which are not readily available in most primary healthcare facilities. As a consequence, several incidents remain undiagnosed, and therapy is often delayed until decompensation. Therefore, there is an urgent need for new biomarkers or biosensing schemes that help to diagnose HF, assess the risk of future events, and guide therapy in community care settings.[2,3]

Common biomarkers in clinical use include markers of neurohumoral activation (NT-pro BNP and BNP) and myocardial damage [cardiac troponin I (cTnI) and cardiac troponin T (cTnT), myocardial isoform of creatine kinase (CK-MB), and myoglobin (Mb)].[4−6] These markers help to differentiate HF from other causes of acute dyspnea in the emergency room as well as to establish short- and long-term prognosis, although their use as a guide for the treatment remains controversial.[7] Despite their usefulness, they fail to

Received: March 8, 2018
Accepted: June 21, 2018
Published: July 9, 2018

DOI: 10.1021/acsami.8b03039
ACS Appl. Mater. Interfaces 2018, 10, 23501−23508

identify consistently high-risk patients who are more likely to benefit from advanced therapies. Several small studies have evaluated the regulation of HF therapy based on BNP-guided therapy with inconsistent results: in a large, recent study performed with patients that presented HF with reduced ejection fraction (HFrEF), the BNP-guided therapy failed to have any effect in reducing rehospitalization or cardiovascular mortality.[8] The limitations of current biomarkers are even more evident for HF with preserved ejection fraction (HFpEF). Subjects with HFpEF are older, more obese than their HFrEF counterparts, and have more comorbidities that may mimic HF as a cause for their symptoms. An approach based only on BNP fails to differentiate HFpEF from exercise deconditioning as a cause of breathlessness in these elderly subjects[9] and may result in falsely reduced values in obese patients.[10] In this scenario, a multimarker approach to assess multiple pathophysiological mechanisms involved in HF is advisable.

Galectin-3 (Gal3), a soluble β-galactosidase-binding glycoprotein released by activated cardiac macrophages, has been proposed as a new cardiac biomarker with unique characteristics.[11−13] Gal3 is responsible for initiating a cascade of profibrotic processes, stimulating the cardiac fibroblasts to deposit collagen into the extracellular matrix, thereby leading to cardiac fibrosis and pathological remodeling of the myocardial structure. Contrary to the natriuretic peptides, Gal3 levels are more stable with time and usher a more malignant course of the disease.[14] Several clinical studies have demonstrated that Gal3 plasma levels higher than 17.8 ng mL^{-1} are associated with a significantly increased risk of hospitalization and death.[15] Moreover, the combination of BNP and Gal3 is superior in predicting mortality compared to either of the biomarkers alone.[16] Information provided by each biomarker may in fact be complementary: in a small study of HF subjects after heart transplantation (HTx), high-sensitivity cTnT measured 10 days after HTx provided prognostic information on survival, whereas Gal3 determined at the same time predicted heart function 1 year after HTx.[17]

To the best of our knowledge, till date, there has been only one novel strategy for the analytical determination of this protein within clinically relevant concentrations.[18] In this recent work, the authors proposed an electrochemical indirect immunoassay method based on a composite made from N-doped graphene nanoribbon-immobilized Fe-based metal−organic frameworks deposited with Au nanoparticles and a primary antibody against Gal3 as the biorecognition element. The sandwich-type electrochemical assay was accomplished by means of a AuPt−methylene blue nanocomposite with a secondary anti-Gal3 antibody. Although the proposed immunosensing strategy presented a linear range from 100 fg mL^{-1} to 50 ng mL^{-1} and a very low detection limit, the assay itself is time-consuming and requires several steps and expensive reagents. Hence, simple, sensitive, and one-step methodologies for Gal3 assessment are highly required, and optical biosensors represent an attractive alternative because of their known advantages and easiness for designing label-free sensing schemes.[19,20]

Surface plasmon resonance (SPR) biosensors, based on the use of modified surfaces with a biomolecule capable of recognizing a given target, have shown promising results in clinical biosensing.[21,22] In this technique, surface plasmon polaritons of a continuous thin Au film are excited by a polarized laser source so that the evanescent wave propagates through the metal/dielectric interface up to hundreds of nanometers.[23] Biosensing strategies based on SPR enable fast, real-time, and label-free analyte detection and provide useful information about binding kinetics and bioaffinity interactions.[24] Current difficulties for SPR-based biosensors are related to the direct detection of analytes at extremely low concentrations or with a small molecular weight.[25] In this sense, the incorporation of plasmonic nanostructures to SPR substrates is an appealing strategy because of the coupled field increments.[26] Graphene-derived materials represent a novel alternative because of the high transmittance of the graphene sheet (97.7%) and the high confinement and high propagation of the surface plasmonic polaritons.[27,28] These advantages, in addition to their high biocompatibility and elevated macromolecule-loading capacity, have made the graphene-derived materials very attractive for the development of SPR biosensors.[29−32]

Recently, we reported a critical study about the noncovalent immobilization of graphene oxide (GO) and modified derivatives (GO and chemically reduced GO) at thiolated Au surfaces as a support for further immobilization of a model protein.[33] We demonstrated that the electrochemical and plasmonic properties of the resulting platforms are related to the nature and quantity of the graphene-derived nanomaterial and the amount of the immobilized protein. Specifically, and for the purpose of the present work, if the transduction method depends on the direct quantification of the amount of protein immobilized at the platform (like SPR), the use of GO is the most appropriate option.

In this work, we report a novel biosensor (to the best of our knowledge, the first optical biosensor) for the important and promising cardiac biomarker, Gal3, using the antibody anti-Gal3 as the biorecognition element and SPR to transduce the immunosensing event. This label-free biosensor is built at thiol-modified Au substrates [Au/sodium 3-mercapto-1-propanesulfonate (MPS)], followed by the layer-by-layer (LBL) self-assembly of poly(diallyldimethyl)ammonium (PDDA) and GO bilayers, covalent attachment of 3-aminephenylboronic acid (3ABA), and immobilization of the antibody. In the following sections, we present the characterization of the starting platform Au/MPS/$(PDDA/GO)_n$ by scanning electron microscopy (SEM), electrochemical scanning microscopy (SECM), and SPR, the SPR study of the immobilization of anti-Gal3, and the final SPR transduction after Gal3 immunosensing. A critical discussion about the effect of GO and 3ABA on the overall performance of the resulting biosensor and the application for the detection of Gal3 in enriched human serum samples is also reported.

2. MATERIALS AND METHODS

2.1. Chemicals and Reagents. GO was obtained from Graphenea. Rat monoclonal anti-Gal3 was purchased from Santa Cruz Biotechnology. Human recombinant Gal3 was received from R&D Systems. PDDA, 3ABA hydrochloride, *N*-(3-dimethylaminopropyl)-*N*′-ethylcarbodiimide hydrochloride (EDC), *N*-hydroxysuccinimide (NHS), ethanolamine ($EtNH_2$), MPS, ferrocene methanol (FcOH), poly(acrylic acid) (PAA), 4-mercaptobenzoic acid (4MBA), and bovine serum albumin (BSA) were purchased from Sigma-Aldrich. Other reagents were of analytical grade and used without further purification. All solutions were prepared with ultrapure water (18 MΩ cm) from a Millipore Milli-Q system.

2.2. Preparation of the Biosensing Surface. The Au SPR disk (BK7) was modified ex situ by covering the surface with a 2.00×10^{-2} M MPS solution (prepared in 1.60×10^{-3} M H_2SO_4) for 60 min. The procedure for assembling PDDA and GO is the same as in our previous work.[33] Briefly, 1.00 mg mL^{-1} PDDA solution was assembled at Au/MPS through interaction for 15 min. After rinsing, the Au/MPS/PDDA

DOI: 10.1021/acsami.8b03039
ACS Appl. Mater. Interfaces 2018, 10, 23501−23508

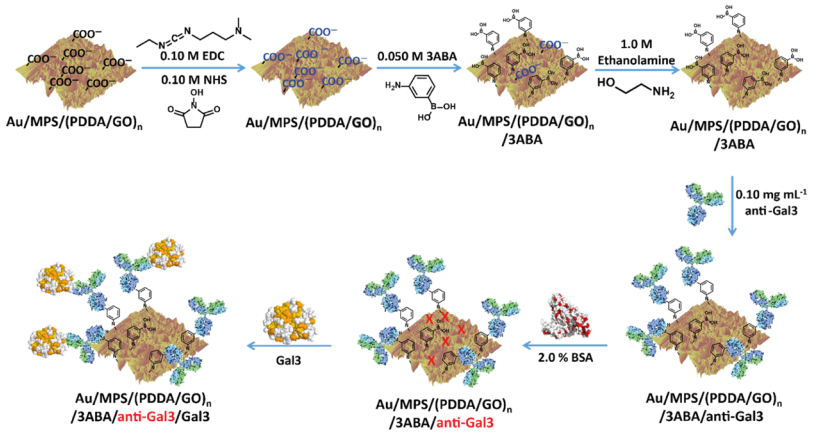

Figure 1. Schematic illustration of the construction of Gal3 immunosensor at the Au/MPS/$(PDDA/GO)_n$ platform.

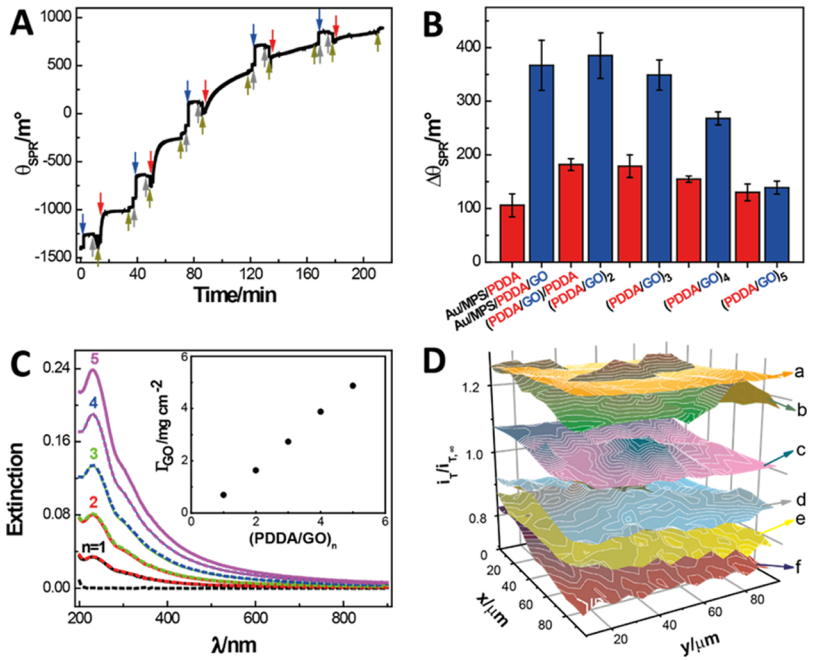

Figure 2. (A) SPR sensorgram obtained during the consecutive LBL self-assembly of five bilayers of 1.00 mg mL^{-1} PDDA (blue arrow) and 0.50 mg mL^{-1} GO (red arrow). Rinsing solutions: 0.050 M phosphate buffer solution pH 7.40 (grey arrow) or water (dark yellow). (B) Change in the SPR angle ($\Delta\theta_{SPR}$) after each adsorption of PDDA or GO at Au/MPS obtained from the SPR sensorgram shown in (A). (C) UV−vis spectra obtained at quartz/$(PDDA/GO)_n$ for n = 1 (black line), 2 (red line), 3 (green line), 4 (blue line), and 5 (magenta line) for the final PDDA (dashed line) or GO (full line) layer. The inset depicts the GO surface coverage (Γ_{GO}) as a function of n, obtained from the final GO layer UV−vis spectra using ε (GO, 230 nm) = 49.0 mL mg^{-1} cm^{-1}. (D) SECM feedback plots obtained at Au/MPS (a) and Au/$(PDDA/GO)_n$ for n = 1 (b), 2 (c), 3 (d), 4 (e), and 5 (f), using 5.00×10^{-4} M FcOH as a redox probe.

surface was allowed to interact with 0.50 mg mL^{-1} GO solution for 30 min. The Au/MPS/$(PDDA/GO)_n$ multilayered system was obtained by repeating these adsorption steps n times.

The immunosensing platform was constructed by following the procedure shown in Figure 1. After the assembly of PDDA/GO multilayers, the carboxylate residues of GO were activated with an EDC/NHS mixture (0.100 M prepared in 0.050 M phosphate buffer solution pH 7.40) for 20 min. After rinsing, the surface was left to interact with 0.050 M 3ABA solution for 30 min to allow the amidation reaction to take place with the amine groups of 3ABA. The unreacted carboxylate groups of GO were quenched by adding 1.0 M $EtNH_2$ solution (the pH was adjusted to 8.30) for 15 min. The anti-Gal3 antibody was immobilized by adding a 0.10 mg mL^{-1} anti-Gal3 solution (prepared in 0.100 M phosphate buffer saline pH 7.40) for 40 min. For blocking the nonspecific adsorption sites, the Au/MPS/$(PDDA/GO)_n$/3ABA/anti-Gal3 platform was left to interact for 30 min with 2.0% BSA solution (prepared in 0.100 M phosphate buffer saline pH 7.40). Finally, the detection of Gal3 was performed by interaction with the protein for 60 min. After Gal3 interaction, the platform was rinsed with 0.100 M phosphate buffer saline pH 7.40 + Tween 0.050 v/v %.

For comparison, the immunosensing platform was also constructed at a gold surface derivatized with 4-mercaptobenzoic acid (4MBA) and at the Au/MPS surface modified with four PDDA/PAA self-assembled bilayers (Figure S1B,C). For the first platform, an Au disk was modified by covering the surface for 60 min with 1.00×10^{-2} M 4MBA ethanolic solution and further rinsing with absolute ethanol and deionized water. For Au/MPS/$(PDDA/PAA)_4$, the self-assembly was performed by four consecutive adsorption cycles as in the case of $(PDDA/GO)_n$, using 1.00 mg mL^{-1} PDDA and 0.50 mg mL^{-1} PAA solutions.

2.3. Apparatus and Procedures. SPR measurements were performed with a single channel Kretschmann configuration Autolab SPRINGLE from Eco Chemie, using BK7 Au sensor disks. Sample solutions (60 μL) were injected manually into the cuvette. All measurements were carried out at (25 ± 1) °C under stagnant

DOI: 10.1021/acsami.8b03039
ACS Appl. Mater. Interfaces 2018, 10, 23501−23508

conditions. Note that in the scanning-angle configuration of the SPRINGLE instrument,[34] the angle scale (y-axis in sensorgrams) is relative and the relevant parameter is the change in the SPR minimum angle ($\Delta\theta_{SPR}$).

SECM images were obtained with a CHI900 bipotentiostat (CHInstruments) using a glass-embedded carbon fiber (diameter ≈ 10 μm) as the ultra-microelectrode (UME) probe. Images in the SECM feedback mode were taken using 5.00×10^{-4} M FcOH as the redox probe. The UME and Au-modified substrate were held at 0.500 and 0.000 V, respectively, and the UME scan rate was 20.0 μm s^{-1}. The SECM surface plots are depicted as the ratio between the UME current at the surface (i_T) and the steady-state one when positioned far from the substrate ($i_{T,\infty}$).

Ultraviolet−visible (UV−vis) experiments were performed with a Shimadzu UV1601 spectrophotometer and a quartz cuvette of 0.1 cm path length. The procedure for activating quartz negative charges for LBL self-assembly is the same as the one described in a previous work.[33]

SEM images were obtained with a field emission gun scanning electron microscope (Zeiss, ΣIGMA model).

3. RESULTS AND DISCUSSION

3.1. Characterization of Au/MPS/(PDDA/GO)$_n$ Films: Optical and Electrochemical Properties and Protein Loading. In this section, we present the optical (SPR and UV−vis spectroscopy), electrochemical (SECM), and microscopy (SEM) characterization of the LBL assembly of (PDDA/GO)$_n$ films at Au/MPS and how this supramolecular architecture affects the surface loading of a model protein for further development of the immunosensing platform.

One of the main advantages of SPR-based platforms is the ability to visualize the immobilization steps/binding events in real time. Figure 2A presents the sensorgram obtained during the self-assembly of five (PDDA/GO) bilayers at Au/MPS. After every assembly step of PDDA or GO, the surface was washed with the corresponding medium, either 0.050 M phosphate buffer solution pH 7.40 or water, respectively. The SPR angle (θ_{SPR}) increases after each adsorption cycle, indicating that there is an effective immobilization of PDDA and GO. Figure 2B depicts the changes in the surface plasmon angle ($\Delta\theta_{SPR}$), taken as the difference of θ_{SPR} before and after the interaction with PDDA or GO and washing of the surface. It can be observed that the increment of $\Delta\theta_{SPR}$ is not the same for each layer, the differences being more evident as n increases, especially in the case of GO. It is important to remark that these changes in the SPR signals during the building of the supramolecular assembly are not due to a limitation of the technique because SPR relies on the propagation of the Au evanescent wave into the solution up to 200 nm, and our platform is far below this value, considering that the thickness per GO assembled layer ranges between 0.85 and 10.9 nm.[35,36] Because SPR is sensitive to changes in the refractive index of the film in contact with the Au surface, the nonregular profile of $\Delta\theta_{SPR}$ with n can be attributed to the immobilization of less amount of material and/or to the change in the optical properties of the successive layers.[30,37] To elucidate this effect, we performed UV−vis experiments after each PDDA and GO adsorption step at an activated quartz cuvette (Figure 2C). Because PDDA does not absorb in the wavelength region under investigation (dashed lines), the surface coverages of GO (Γ_{GO}) can be obtained directly from the GO extinction maxima at 230 nm (full lines) because of the $\pi-\pi^*$ transition of the conjugated C=C bonds. The linear variation of Γ_{GO} with the number of (PDDA/GO) bilayers (showed in the inset) indicates that the amount of GO immobilized is proportional to n, in agreement with other reported GO self-assemblies.[35,38] These results demonstrate that the nonuniform variation of $\Delta\theta_{SPR}$ with (PDDA/GO)$_n$ is due to the change in the optical properties of the successive layers and not due to the immobilization of a smaller amount of PDDA/GO. Figure 2D displays the SECM profiles obtained at Au/MPS/(PDDA/GO)$_n$ using FcOH as a redox mediator. There is a decrease in the average $i_T/i_{T,\infty}$ with the increase of n, indicating a more difficult charge transfer of FcOH as the amount of PDDA/GO at the electrode surface increases, as expected considering that GO-modified electrodes are characterized by slow electron-transfer processes (see also Table S1). The change of average $i_T/i_{T,\infty}$ with the number of PDDA/GO bilayers presents a trend similar to the one observed for $\Delta\theta_{SPR}$, although the effect is less pronounced.

The SEM images displayed in Figure S2 for Au/MPS/(PDDA/GO)$_n$ with n = 1−5 reveal that the supramolecular architecture grows irregularly in terms of Au coverage. Au/MPS/(PDDA/GO) and Au/MPS/(PDDA/GO)$_2$ images show some regions with uncovered Au surface, whereas for n > 3, the surface tends to be fully covered. Considering that the deposited mass of GO after each step is almost constant, these results indicate that for low n, the electrochemical and plasmonic properties change as a consequence of the incomplete Au coating, in agreement with the abrupt changes in $i_T/i_{T,\infty}$. As n increases, the platform presents the final properties of a fully GO-exposed surface, once again following the less pronounced changes in $i_T/i_{T,\infty}$. This nonuniform change in the platform properties with increasing number of GO films deposited is due to its high aspect ratio, which causes interpenetration of the successive layers, as already suggested in other studies.[39,40]

Because the goal of optimization of Au/MPS/(PDDA/GO)$_n$ is to maximize the capacity for immobilizing a biosensing protein, we evaluated by SPR the immobilization of BSA, as a model protein, by covalent attachment at Au/MPS/(PDDA/GO)$_n$ through EDC/NHS chemistry. Figure S3 presents the variation of BSA surface coverage (Γ_{BSA}) at Au/MPS/(PDDA/GO)$_n$ as a function of n (obtained from independent experiments). Γ_{BSA} grows with (PDDA/GO)$_n$ until n = 4 and remains almost constant thereafter. Considering the SECM and SEM results previously described and the Γ_{BSA} versus n plot, the interpenetration of GO sheets with the increment of n is highly probable,[39] reducing the availability of carboxylate anchoring points of the platform able to bind the protein, and consequently, Γ_{BSA} stops to increase. It is interesting to note that Γ_{BSA} does not follow the same trend as Γ_{GO}, indicating that the protein loading depends on the final structure of the resulting Au/MPS/(PDDA/GO)$_n$ supramolecular architecture and is not proportional to the amount of assembled GO. Therefore, the platform selected for the construction of the Gal3 immunosensor is Au/MPS/(PDDA/GO)$_4$.

3.2. Construction of the Immunosensing Platform: Au/MPS/(PDDA/GO)$_4$/3ABA/Anti-Gal3. Figure 3A shows the SPR profiles obtained during the assembly of the immunosensing platform at Au/MPS/(PDDA/GO)$_4$. The building starts with the activation of GO −COOH groups through the EDC/NHS chemistry, followed by the derivatization with 3ABA, quenching of nonreacted −COOH groups with $EtNH_2$ before the oriented binding of anti-Gal3 to the platform, and blocking of nonspecific adsorption sites with the BSA concentrated solution. The analytical signal was obtained from the change in θ_{SPR} before and after Gal3 addition and rinsing with Tween + buffer solution (inset of Figure 3A). In this particular case, after addition of 50.0 mg mL^{-1} Gal3, $\Delta\theta_{SPR}$ was (85 ± 5) m°.

DOI: 10.1021/acsami.8b03039
ACS Appl. Mater. Interfaces 2018, 10, 23501−23508

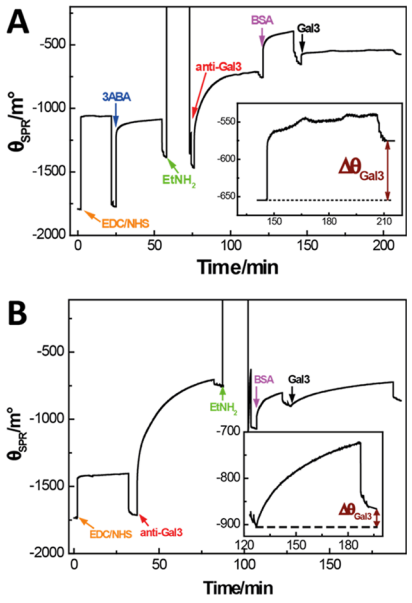

Figure 3. (A) SPR sensorgram obtained during the activation of Au/MPS/$(PDDA/GO)_4$ with EDC/NHS (orange arrow), covalent immobilization of 3ABA (blue arrow), quenching with $EtNH_2$ (green arrow), oriented binding of anti-Gal3 (red arrow), blocking of nonspecific adsorption sites with 2.0% BSA (magenta arrow), and interaction with Gal3 target (black arrow). The inset shows $\Delta\theta_{SPR}$ obtained after addition of Gal3, used as the analytical signal. (B) SPR sensorgram obtained during the activation of Au/MPS/$(PDDA/GO)_4$ with EDC/NHS (orange arrow), covalent immobilization of anti-Gal3 (red arrow), quenching with $EtNH_2$ (green arrow), blocking of nonspecific adsorption sites with the BSA concentrated solution (magenta arrow), and interaction with Gal3 target (black arrow). The insets show the response to Gal3 in different scales.

Before discussing the analytical performance of the resulting immunosensor, it is relevant to demonstrate the importance of using 3ABA to orientate the immobilization of the biorecognition element. It is known that boronic acid can bind moieties with 1,2- or 1,3-cis-diol groups and form five or six-membered cyclic boronate esters (Figure S4).[41] Therefore, considering that antibodies present an oligosaccharide residue in the Fc region and in order to preserve the biological activity of anti-Gal3 and improve the sensitivity of the biosensor,[42] we used 3ABA to orientate the antibody tethered to the platform. We also compared the interaction of Gal3 with a platform obtained by direct immobilization of anti-Gal3 through EDC/NHS chemistry without site-specific binding [Au/MPS/$(PDDA/GO)_4$/anti-Gal3]. Figure 3B shows the sensorgram for the direct immobilization of anti-Gal3 at Au/MPS/$(PDDA/GO)_4$ and the interaction of the resulting platform with 50.0 ng mL^{-1} Gal3. $\Delta\theta_{SPR}$ after interacting with Gal3 was (40 ± 6) m°, that is, less than the half of the signal obtained at Au/MPS/$(PDDA/GO)_4$/3ABA/anti-Gal3 (Figure 3A), demonstrating that boronic acid-saccharide-mediated immobilization of anti-Gal3 provides a more efficient biosensing performance. Anti-Gal3 surface coverage($\Gamma_{anti\text{-}Gal3}$) for the oriented and non-oriented strategies, obtained from the corresponding$\Delta\theta_{SPR}$, were (5.91 ± 0.08) × 10^{-4} and (7.9 ± 0.1) × 10^{-4} mg cm^{-2}, respectively. This reinforces the fact that the increase in the signal after adding Gal3 when 3ABA is present is not due to an increment in the amount of immobilized anti-Gal3, because $\Gamma_{anti\text{-}Gal3}$ at Au/MPS/$(PDDA/GO)_4$ is even higher than at Au/MPS/$(PDDA/GO)_4$/3ABA.

At this point, it is relevant to evaluate the importance of the presence of GO on the performance of the bioanalytical platform. To clarify this matter, we assayed the immobilization of 3ABA at another source of carboxylate groups, that is, a self-assembled monolayer of 4MBA thiol (the scheme is shown in Figure S1B). 3ABA was covalently attached to Au/4MBA through the carboxylate residues of 4MBA. Figure 4A displays the response of Au/MPS/$(PDDA/GO)_4$/3ABA and Au/4MBA/3ABA during the immobilization of anti-Gal3. $\Delta\theta_{SPR}$ obtained after binding anti-Gal3 to Au/4MBA/3ABA was 22 times smaller than $\Delta\theta_{SPR}$ at Au/MPS/$(PDDA/GO)_4$/3ABA (Figure 4A). As a consequence of this poor immobilization of anti-Gal3 at Au/4MBA/3ABA, further addition of 50.0 ng mL^{-1} Gal3 (Figure 4B) shows almost no $\Delta\theta_{SPR}$. The amplification effect of GO on θ_{SPR} can be due to two factors: (i), the increase of the attached biomolecules (anti-Gal3 in this case) due to its large surface area and the high carboxylate residue density; and (ii), the increase of the electromagnetic field.[43,44] To know which is the prevalent effect, PDDA multilayers were assembled with PAA instead of GO (the scheme is shown in Figure S1C). The selection of PAA was made taking into account that it has a density of 1.39 × 10^{-5} mol of carboxylate groups per mg of material, almost 4 times higher than that of GO (3.81 × 10^{-6} mol of −COOH per mg of material). SPR experiments demonstrate that the self-assembly of $(PDDA/PAA)_4$ at Au/MPS immobilizes 2.19 μg cm^{-2} of PAA, which gives a −COOH surface density of 30.9 nmol cm^{-2}, whereas at Au/MPS/$(PDDA/GO)_4$, the −COOH surface density is 14.8 nmol cm^{-2}. Figure S5 shows the sensorgrams obtained for the immobilization of anti-Gal3 and Gal3 at Au/MPS/$(PDDA/PAA)_4$/3ABA using the same conditions as those for the GO-based immunosensor. $\Delta\theta_{SPR}$ of (85 ± 3) and (14 ± 2) m° were obtained after interaction with anti-Gal3 and Gal3, respectively. Thus, upon antibody binding

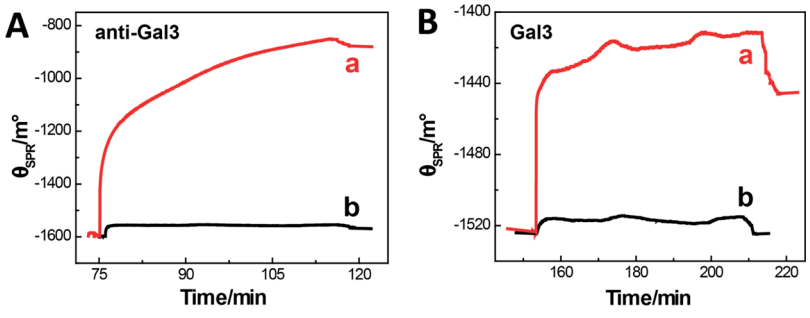

Figure 4. SPR sensorgrams for the immobilization of anti-Gal3 (A) and Gal3 target (B) at Au/MPS/$(PDDA/GO)_4$/3ABA (a) and Au/4MBA/3ABA (b) platforms. Other conditions and concentrations as in section 2.2.

DOI: 10.1021/acsami.8b03039
ACS Appl. Mater. Interfaces 2018, 10, 23501−23508

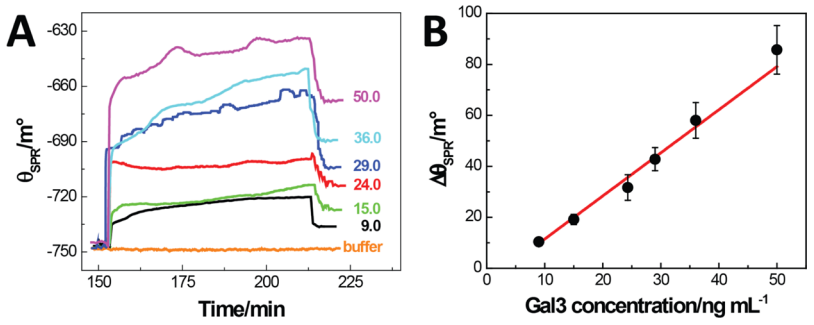

Figure 5. (A) SPR sensorgrams obtained at Au/MPS/$(PDDA/GO)_4$/3ABA/anti-Gal3 for the addition of different concentrations of Gal3: 9.0, 15.0, 24.0, 36.0, and 50.0 ng mL^{-1}. Each sensorgram corresponds to an independent experiment. (B) Calibration plot for Gal3 quantification. Each point is an average of three different experiments.

at the higher −COOH density surface Au/MPS/$(PDDA/PAA)_4$/3ABA, it gives a signal even 8.4 times smaller, demonstrating that the main effect of GO is the increase of sensitivity due to its optical properties.

Another important aspect to evaluate when developing a biosensing platform is the nonspecific adsorption of the target. To demonstrate that the response for Gal3 is only due to immune recognition, a control experiment was performed at a surface without the antibody (Au/MPS/$(PDDA/GO)_4$/3ABA) (Figure S6). After quenching 3ABA sites with ethylene glycol and blocking nonspecific sites with BSA, $\Delta\theta_{SPR}$ obtained for the addition of 50.0 ng mL^{-1} Gal3 was minimum, showing a negligible unspecific interaction of Gal3 with the platform.

3.3. Analytical Performance of the Gal3 Immunosensor. Figure 5A presents the sensorgrams for the addition of different concentrations of Gal3. The plot of $\Delta\theta_{SPR}$ as a function of Gal3 concentration (Figure 5B) shows a linear dependency between 10.0 and 50.0 ng mL^{-1}, with a detection limit of 2.0 ng mL^{-1} (taken as 3.3 times the standard deviation of the blank signal divided by the sensitivity). Even when the detection limit is higher than the one recently proposed for the electrochemical quantification of Gal3,[18] our biosensor offers the advantage of a faster one-step detection with a linear range that includes Gal3-relevant clinical concentrations (17.8−25.9 ng mL^{-1}) comparable to the commercially available enzyme-linked immunosorbent assay kit.[45,46]

The selectivity of the designed biosensor was examined through the interaction of the biosensing platform with the main proteins present in human serum: 40.0 mg mL^{-1} human serum albumin, 15.0 mg mL^{-1} immunoglobulin G (IgG), 150.0 mg mL^{-1} haemoglobin, and 3.0 mg mL^{-1} transferrin (Figure S7). The interference percentages of the different proteins relative to $\Delta\theta_{SPR}$ for 50.0 ng mL^{-1} Gal3 addition were 0.3, 11.4, 0.0, and 1.2%, respectively. The results indicate that the platform is highly selective, with interference percentages acceptable from the analytical point of view, especially considering that these serum proteins were added in a huge excess compared to Gal3 (mg mL^{-1} vs ng mL^{-1}, respectively).

To evaluate the usefulness of Au/MPS/$(PDDA/GO)_4$/3ABA/anti-Gal3 bioplatform for further analytical applications, we performed recovery assays using 1:3 diluted human serum samples enriched with 30.0 ng mL^{-1} Gal3. The recovery of Gal3 SPR signal was 108%, showing that our biosensor could be used for early determination of cardiovascular disease risk in clinical laboratory real samples.

4. CONCLUSIONS

In summary, we reported the first optical biosensor for the quantification of the new cardiac biomarker Gal3 using the antibody anti-Gal3 as the biorecognition element and the GO-enhanced SPR methology for transducing the immunological interaction. We presented a critical evaluation of the basic platform, Au/MPS/$(PDDA/GO)_4$, as the initial step in the construction of the immunosensing layer, demonstrating the advantages of using GO in its double role of antibody anchor point and amplifier of the SPR response and 3ABA as the orientating element for the biorecognition molecule. In fact, the role of GO as the enhancer of the analytical signal makes our biosensing scheme highly advantageous because the amplification is attained in the starting platform without any postamplification step once the antibody−antigen reaction occurred, and the use of 3ABA highly contributes to enhancing the specificity of the anti-Gal3 platform. The resulting biosensor proved to be useful for the highly sensitive and selective label-free detection of Gal3 in the whole range of clinically relevant concentrations, with successful application for the quantification in enriched human serum samples. The new design represents a competitive alternative for the quantification of this new and important cardiac biomarker.

■ ASSOCIATED CONTENT

Supporting Information

The Supporting Information is available free of charge on the ACS Publications website at DOI: 10.1021/acsami.8b03039.

Schematic illustrations of platforms and reactions, average $i_T/i_{T,\infty}$ values from Figure 2D, SEM images of Au/MPS/$(PDDA/GO)_n$, model protein surface coverage (Γ_{BSA}) as a function of the number of $(PDDA/GO)_n$ bilayers, and sensorgrams for Au/MPS/$(PDDA/PAA)_4$/3ABA platform and for selectivity and specific binding experiments (PDF)

■ AUTHOR INFORMATION

Corresponding Authors

*E-mail: sbollo@ciq.uchile.cl (S.B.).
*E-mail: rubianes@fcq.unc.edu.ar (M.D.R.).
*E-mail: grivas@fcq.unc.edu.ar (G.A.R.).

ORCID

Gustavo A. Rivas: 0000-0001-7411-6821

Notes

The authors declare no competing financial interest.

DOI: 10.1021/acsami.8b03039
ACS Appl. Mater. Interfaces 2018, 10, 23501−23508

■ ACKNOWLEDGMENTS

Financial support from CONICET, ANPCyT, SECyT-UNC (Argentina), and National Fund for Scientific and Technological Development-CHILE FONDECYT no. 1161225 and FONDAP no. 15130011 are gratefully acknowledged. E.N.P. thankfully acknowledges CONICET for the PhD fellowship.

■ REFERENCES

(1) Mozaffarian, D.; Benjamin, E. J.; Go, A. S.; Arnett, D. K.; Blaha, M. J.; Cushman, M.; Das, S. R.; de Ferranti, S.; Després, J.-P.; Fullerton, H. J.; Howard, V. J.; Huffman, M. D.; Isasi, C. R.; Jiménez, M. C.; Judd, S. E.; Kissela, B. M.; Lichtman, J. H.; Lisabeth, L. D.; Liu, S.; Mackey, R. H.; Magid, D. J.; McGuire, D. K.; Mohler, E. R.; Moy, C. S.; Muntner, P.; Mussolino, M. E.; Nasir, K.; Neumar, R. W.; Nichol, G.; Palaniappan, L.; Pandey, D. K.; Reeves, M. J.; Rodriguez, C. J.; Rosamond, W.; Sorlie, P. D.; Stein, J.; Towfighi, A.; Turan, T. N.; Virani, S. S.; Woo, D.; Yeh, R. W.; Turner, M. B. Heart Disease and Stroke Statistics—2016 Update. *Circulation* **2016**, *133*, e38−360.

(2) Chow, S. L.; Maisel, A. S.; Anand, I.; Bozkurt, B.; de Boer, R. A.; Felker, G. M.; Fonarow, G. C.; Greenberg, B.; Januzzi, J. L.; Kiernan, M. S.; Liu, P. P.; Wang, T. J.; Yancy, C. W.; Zile, M. R. Role of Biomarkers for the Prevention, Assessment, and Management of Heart Failure: A Scientific Statement From the American Heart Association. *Circulation* **2017**, *135*, e1054−e1091.

(3) Moayedi, Y.; Ross, H. J. Advances in Heart Failure: A Review of Biomarkers, Emerging Pharmacological Therapies, Durable Mechanical Support and Telemonitoring. *Clin. Sci.* **2017**, *131*, 553−566.

(4) Abdorahim, M.; Rabiee, M.; Alhosseini, S. N.; Tahriri, M.; Yazdanpanah, S.; Alavi, S. H.; Tayebi, L. Nanomaterials-Based Electrochemical Immunosensors for Cardiac Troponin Recognition: An Illustrated Review. *TrAC, Trends Anal. Chem.* **2016**, *82*, 337−347.

(5) Justino, C. I. L.; Duarte, A. C.; Rocha-Santos, T. A. P. Critical Overview on the Application of Sensors and Biosensors for Clinical Analysis. *TrAC, Trends Anal. Chem.* **2016**, *85*, 36−60.

(6) Rezaei, B.; Ghani, M.; Shoushtari, A. M.; Rabiee, M. Electrochemical Biosensors Based on Nanofibres for Cardiac Biomarker Detection: A Comprehensive Review. *Biosens. Bioelectron.* **2016**, *78*, 513−523.

(7) Onda, T.; Inoue, K.; Suwa, S.; Nishizaki, Y.; Kasai, T.; Kimura, Y.; Fukuda, K.; Okai, I.; Fujiwara, Y.; Matsuoka, J.; Sumiyoshi, M.; Daida, H. Reevaluation of Cardiac Risk Scores and Multiple Biomarkers for the Prediction of First Major Cardiovascular Events and Death in the Drug-Eluting Stent Era. *Int. J. Cardiol.* **2016**, *219*, 180−185.

(8) Felker, G. M.; Anstrom, K. J.; Adams, K. F.; Ezekowitz, J. A.; Fiuzat, M.; Houston-Miller, N.; Januzzi, J. L., Jr.; Mark, D. B.; Piña, I. L.; Passmore, G.; Whellan, D. J.; Yang, H.; Cooper, L. S.; Leifer, E. S.; Desvigne-Nickens, P.; O'Connor, C. M. Effect of Natriuretic Peptide−guided Therapy on Hospitalization or Cardiovascular Mortality in High-Risk Patients with Heart Failure and Reduced Ejection Fraction: A Randomized Clinical Trial. *JAMA, J. Am. Med. Assoc.* **2017**, *318*, 713−720.

(9) Parasuraman, S. K.; Singh, S.; Schwarz, K.; Rudd, A.; Dawson, D.; Frenneaux, M. P. Abstract 19271: Resting and Post Exercise Serum Brain Natriuretic Peptide Levels Do Not Help Differentiate Heart Failure With Normal Ejection Fraction From Respiratory Limitation and Deconditioning in Patients Aged Over 60 Years. *Circulation* **2016**, *134*, A19271.

(10) Madamanchi, C.; Alhosaini, H.; Sumida, A.; Runge, M. S. Obesity and Natriuretic Peptides, BNP and NT-ProBNP: Mechanisms and Diagnostic Implications for Heart Failure. *Int. J. Cardiol.* **2014**, *176*, 611−617.

(11) Agnello, L.; Bivona, G.; Lo Sasso, B.; Scazzone, C.; Bazan, V.; Bellia, C.; Ciaccio, M. Galectin-3 in Acute Coronary Syndrome. *Clin. Biochem.* **2017**, *50*, 797−803.

(12) Henderson, N. C.; Sethi, T. The Regulation of Inflammation by Galectin-3. *Immunol. Rev.* **2009**, *230*, 160−171.

(13) Sharma, U. C.; Pokharel, S.; van Brakel, T. J.; van Berlo, J. H.; Cleutjens, J. P. M.; Schroen, B.; André, S.; Crijns, H. J. G. M.; Gabius, H.-J.; Maessen, J.; Pinto, Y. M. Galectin-3 Marks Activated Macrophages in Failure-Prone Hypertrophied Hearts and Contributes to Cardiac Dysfunction. *Circulation* **2004**, *110*, 3121−3128.

(14) Lok, D. J.; Lok, S. I.; de la Porte, P. W. B.-A.; Badings, E.; Lipsic, E.; van Wijngaarden, J.; de Boer, R. A.; van Veldhuisen, D. J.; van der Meer, P. Galectin-3 Is an Independent Marker for Ventricular Remodeling and Mortality in Patients with Chronic Heart Failure. *Clin. Res. Cardiol.* **2013**, *102*, 103−110.

(15) Shah, R. V.; Januzzi, J. L. Soluble ST2 and Galectin-3 in Heart Failure. *Clin. Lab. Med.* **2014**, *34*, 87−97.

(16) Srivatsan, V.; George, M.; Shanmugam, E. Utility of Galectin-3 as a Prognostic Biomarker in Heart Failure: Where Do We Stand? *Eur. J. Prev. Cardiol.* **2014**, *22*, 1096−1110.

(17) Franeková, J.; Hošková, L.; Sečník, P.; Pazderník, M.; Kotrbatá, M.; Kubíček, Z.; Jabor, A. The Role of Timely Measurement of Galectin-3, NT-ProBNP, Cystatin C and HsTnT in Predicting Prognosis and Heart Function after Heart Transplantation. *Clin. Chem. Lab. Med.* **2016**, *54*, 339−344.

(18) Tang, Z.; He, J.; Chen, J.; Niu, Y.; Zhao, Y.; Zhang, Y.; Yu, C. A Sensitive Sandwich-Type Immunosensor for the Detection of Galectin-3 Based on N-GNRs-Fe-MOFs@AuNPs Nanocomposites and a Novel AuPt-Methylene Blue Nanorod. *Biosens. Bioelectron.* **2018**, *101*, 253−259.

(19) Felix, F. S.; Angnes, L. Electrochemical Immunosensors − A Powerful Tool for Analytical Applications. *Biosens. Bioelectron.* **2018**, *102*, 470−478.

(20) Khansili, N.; Rattu, G.; Krishna, P. M. Label-Free Optical Biosensors for Food and Biological Sensor Applications. *Sens. Actuators, B* **2018**, *265*, 35−49.

(21) Puiu, M.; Bala, C. SPR and SPR Imaging: Recent Trends in Developing Nanodevices for Detection and Real-Time Monitoring of Biomolecular Events. *Sensors* **2016**, *16*, 870.

(22) Singh, P. SPR Biosensors: Historical Perspectives and Current Challenges. *Sens. Actuators, B* **2016**, *229*, 110−130.

(23) Kooyman, R. P. H. Physics of Surface Plasmon Resonance. In *Handbook of Surface Plasmon Resonance*; Tudos, A. J., Schasfoort, R. B. M., Eds.; The Royal Society of Chemistry: Cambridge, 2008; Chapter 2, pp 15−34.

(24) Masson, J.-F. Surface Plasmon Resonance Clinical Biosensors for Medical Diagnostics. *ACS Sens.* **2017**, *2*, 16−30.

(25) Snopok, B. A. Theory and Practical Application of Surface Plasmon Resonance for Analytical Purposes. *Theor. Exp. Chem.* **2012**, *48*, 283−306.

(26) Zeng, S.; Baillargeat, D.; Ho, H.-P.; Yong, K.-T. Nanomaterials Enhanced Surface Plasmon Resonance for Biological and Chemical Sensing Applications. *Chem. Soc. Rev.* **2014**, *43*, 3426−3452.

(27) Grigorenko, A. N.; Polini, M.; Novoselov, K. S. Graphene Plasmonics. *Nat. Photonics* **2012**, *6*, 749−758.

(28) Jung, I.; Rhyee, J.-S.; Son, J. Y.; Ruoff, R. S.; Rhee, K.-Y. Colors of Graphene and Graphene-Oxide Multilayers on Various Substrates. *Nanotechnology* **2012**, *23*, 025708.

(29) He, L.; Pagneux, Q.; Larroulet, I.; Serrano, A. Y.; Pesquera, A.; Zurutuza, A.; Mandler, D.; Boukherroub, R.; Szunerits, S. Label-Free Femtomolar Cancer Biomarker Detection in Human Serum Using Graphene-Coated Surface Plasmon Resonance Chips. *Biosens. Bioelectron.* **2017**, *89*, 606−611.

(30) Shynkarenko, O. V.; Kravchenko, S. A. Surface Plasmon Resonance Sensors: Methods of Surface Functionalization and Sensitivity Enhancement. *Theor. Exp. Chem.* **2015**, *51*, 273−292.

(31) Vasilescu, A.; Gáspár, S.; Gheorghiu, M.; David, S.; Dinca, V.; Peteu, S.; Wang, Q.; Li, M.; Boukherroub, R.; Szunerits, S. Surface Plasmon Resonance Based Sensing of Lysozyme in Serum on Micrococcus Lysodeikticus-Modified Graphene Oxide Surfaces. *Biosens. Bioelectron.* **2017**, *89*, 525−531.

(32) Yao, T.; Gu, X.; Li, T.; Li, J.; Li, J.; Zhao, Z.; Wang, J.; Qin, Y.; She, Y. Enhancement of Surface Plasmon Resonance Signals Using a MIP/GNPs/RGO Nano-Hybrid Film for the Rapid Detection of Ractopamine. *Biosens. Bioelectron.* **2016**, *75*, 96−100.

DOI: 10.1021/acsami.8b03039
ACS Appl. Mater. Interfaces 2018, 10, 23501−23508

(33) Primo, E. N.; Bollo, S.; Rubianes, M. D.; Rivas, G. A. Immobilization of Graphene-Derived Materials at Gold Surfaces: Towards a Rational Design of Protein-Based Platforms for Electrochemical and Plasmonic Applications. *Electrochim. Acta* **2018**, *259*, 723−732.
(34) Schasfoort, R. B. M. Surface Plasmon Resonance Instruments. *Handbook of Surface Plasmon Resonance*; The Royal Society of Chemistry, 2017; Chapter 3, pp 60−105.
(35) Heo, J.; Choi, M.; Chang, J.; Ji, D.; Kang, S. W.; Hong, J. Highly Permeable Graphene Oxide/Polyelectrolytes Hybrid Thin Films for Enhanced CO2/N2 Separation Performance. *Sci. Rep.* **2017**, *7*, 456.
(36) Zhao, J.; Zhu, Y.; Pan, F.; He, G.; Fang, C.; Cao, K.; Xing, R.; Jiang, Z. Fabricating Graphene Oxide-Based Ultrathin Hybrid Membrane for Pervaporation Dehydration via Layer-by-Layer Self-Assembly Driven by Multiple Interactions. *J. Membr. Sci.* **2015**, *487*, 162−172.
(37) Ekgasit, S.; Tangcharoenbumrungsuk, A.; Yu, F.; Baba, A.; Knoll, W. Resonance Shifts in SPR Curves of Nonabsorbing, Weakly Absorbing, and Strongly Absorbing Dielectrics. *Sens. Actuators, B* **2005**, *105*, 532−541.
(38) Huang, D.; Zhang, B.; Zhang, Y.; Zhan, F.; Xu, X.; Shen, Y.; Wang, M. Electrochemically Reduced Graphene Oxide Multilayer Films as Metal-Free Electrocatalysts for Oxygen Reduction. *J. Mater. Chem. A* **2013**, *1*, 1415−1420.
(39) Sham, A. Y. W.; Notley, S. M. Layer-by-Layer Assembly of Thin Films Containing Exfoliated Pristine Graphene Nanosheets and Polyethyleneimine. *Langmuir* **2014**, *30*, 2410−2418.
(40) Shao, J.-J.; Lv, W.; Yang, Q.-H. Self-Assembly of Graphene Oxide at Interfaces. *Adv. Mater.* **2014**, *26*, 5586−5612.
(41) Wu, X.; Chen, X.-X.; Jiang, Y.-B. Recent Advances in Boronic Acid-Based Optical Chemosensors. *Analyst* **2017**, *142*, 1403−1414.
(42) Duval, F.; van Beek, T. A.; Zuilhof, H. Key Steps towards the Oriented Immobilization of Antibodies Using Boronic Acids. *Analyst* **2015**, *140*, 6467−6472.
(43) Chiu, N.-F.; Huang, T.-Y. Sensitivity and Kinetic Analysis of Graphene Oxide-Based Surface Plasmon Resonance Biosensors. *Sens. Actuators, B* **2014**, *197*, 35−42.
(44) Wu, L.; Guo, J.; Wang, Q.; Lu, S.; Dai, X.; Xiang, Y.; Fan, D. Sensitivity Enhancement by Using Few-Layer Black Phosphorus-Graphene/TMDCs Heterostructure in Surface Plasmon Resonance Biochemical Sensor. *Sens. Actuators, B* **2017**, *249*, 542−548.
(45) Felker, G. M.; Fiuzat, M.; Shaw, L. K.; Clare, R.; Whellan, D. J.; Bettari, L.; Shirolkar, S. C.; Donahue, M.; Kitzman, D. W.; Zannad, F.; Piña, I. L.; O'Connor, C. M. Galectin-3 in Ambulatory Patients With Heart Failure: Results From the HF-ACTION Study. *Circ.: Heart Failure* **2012**, *5*, 72−78.
(46) Grandin, E. W.; Jarolim, P.; Murphy, S. A.; Ritterova, L.; Cannon, C. P.; Braunwald, E.; Morrow, D. A. Galectin-3 and the Development of Heart Failure after Acute Coronary Syndrome: Pilot Experience from PROVE IT-TIMI 22. *Clin. Chem.* **2012**, *58*, 267−273.

DOI: 10.1021/acsami.8b03039
ACS Appl. Mater. Interfaces 2018, 10, 23501−23508